PHYSICAL REVIEW B **88**, 205208 (2013)

Strong anisotropy of momentum-relaxation time induced by intermolecular vibrations of single-crystal organic semiconductors

Hiroyuki Ishii,[1,2,*] Nobuhiko Kobayashi,[1] and Kenji Hirose[3]
[1]*Institute of Applied Physics, Tsukuba Research Center for Interdisciplinary Materials Science, University of Tsukuba, 1-1-1 Tennodai, Tsukuba, Ibaraki 305-8573, Japan*
[2]*JST-PRESTO, University of Tsukuba, 1-1-1 Tennodai, Tsukuba, Ibaraki 305-8573, Japan*
[3]*Green Innovation Research Laboratories, NEC Corporation, 34 Miyukigaoka, Tsukuba, Ibaraki 305-8501, Japan*
(Received 12 June 2013; revised manuscript received 25 October 2013; published 20 November 2013)

We present a theoretical study of the relationships between intermolecular vibrations and anisotropic transport properties of pentacene and rubrene single-crystal organic semiconductors. Using our wave-packet approach based on the Kubo formula beyond the effective-mass approximation with the assumption of an isotropic momentum-relaxation time, we find that the intermolecular vibrations induce a strong anisotropic momentum-relaxation time but moderate the anisotropy of carrier mobility much more than that of the effective mass. This clarifies the mechanism behind the deviation of the anisotropic ratio of mobility from that of effective mass observed in angle-resolved photoelectron spectroscopy experiments.

DOI: 10.1103/PhysRevB.88.205208 PACS number(s): 72.80.Le, 73.50.−h

Understanding carrier transport coupled with molecular vibrations in organic semiconductors is the key to not only progress in basic material science, but also their application to flexible devices, such as transistors,[1–3] light-emitting diodes,[4] and solar cells.[5] Organic single crystals are unique and invaluable materials for the study of intrinsic charge transport properties of organic materials free from many morphological issues. Recent progress in technology enables us to fabricate single-crystal organic semiconductors and to construct flexible thin-film transistors with high carrier mobilities of up to $\sim$40 cm^2 V^{-1} s^{-1}.[3]

The molecular design of organic materials is essential for obtaining flexible devices with improved performance. In this respect, it is important to investigate the relationships of "anisotropic" transport properties with the molecular packing structure, intermolecular electronic coupling, and molecular vibration. The anisotropy of carrier mobility μ was observed in experiments on some organic single crystals.[6–11] Angle-resolved photoelectron spectroscopy clarified that the effective-mass tensor m^*, derived from the anisotropic electronic band dispersion, has strong correlations with transport properties in the effective-mass approximation, i.e., $\mu = e\tau/m^*$, where τ is the isotropic momentum-relaxation time.[12] These results are also supported by theoretical studies based on density functional calculations.[13–15] However, although the directions of the highest and lowest mobilities agree with those of the inverse effective mass, the anisotropic ratio of mobilities defined by $\mu_{\max}/\mu_{\min}$ deviates significantly from the ratio of the effective mass $m^*_{\max}/m^*_{\min}$.

Beyond the simple effective-mass approximation, the origin of the anisotropic transport properties has been discussed over the past decade. In the framework of the hopping transport mechanism, the Marcus theory[16–18] is often employed but suffers from apparent differences between the calculated and the observed mobility ratio $\mu_{\max}/\mu_{\min}$ in experiments. Using the Kubo formula, Ortmann *et al.* performed an analytical evaluation of the mobility of carriers coupled with molecular vibrations within the polaron quasiparticle picture.[19] They studied the anisotropy of polaron mobility under the assumption of an isotropic momentum-relaxation time originating from the static disorder. Troisi discussed the effects of intermolecular vibration on the two-dimensional transport properties of rubrene using wave-packet dynamics.[20] Since he assumed that a single molecule in the crystal vibrates at a single frequency without interactions with the neighboring molecules, the intermolecular vibrations are different from a realistic lattice phonon with a continuum spectrum.

To take into account the realistic intermolecular-vibration (lattice-phonon) effects without the assumption of an isotropic momentum-relaxation time, we perform systematic studies on the anisotropic charge transport properties due to the intermolecular-vibration effects. We use the quantum wave-packet dynamical approach based on the Kubo formula for the transport, taking both the realistic molecular packing structures of single-crystal pentacene and rubrene and the intermolecular vibrations into account. We find that intermolecular vibrations induce strong anisotropy of the momentum-relaxation time but moderate the anisotropic nature of carrier mobilities much more than that of the effective mass. Moreover, we find that the anisotropic mobilities exhibit apparent temperature dependence.

The transport properties of molecular crystals are evaluated on the basis of the Kubo formula with the use of the quantum-mechanical calculations of electron wave-packet dynamics combined with a molecular dynamics simulation.[21] The time dependence of the carrier mobility along the ξ axis of a material with volume Ω is written as

$$\mu_\xi = \lim_{t\to+\infty} \frac{e}{n} \int_{-\infty}^{+\infty} dE \left(-\frac{df(E)}{dE}\right) \times \left\langle \frac{\delta(E-\hat{H}_e)}{\Omega} \frac{\{\hat{\xi}(t)-\hat{\xi}(0)\}^2}{t} \right\rangle, \tag{1}$$

where the carrier concentration is defined by $n = \int dE\, f(E)\nu(E)$ with the density of states (DOS) $\nu(E)$ and the Fermi distribution function $f(E)$. The position operator of charge is written as $\hat{\xi}(t) \equiv \hat{U}^\dagger(t)\hat{\xi}\hat{U}(t)$ with $\hat{U}(t = N_t\Delta t) \equiv \Pi_{n=0}^{N_t-1} \exp\{i\hat{H}_e(n\,\Delta t)\Delta t/\hbar\}$ in the Heisenberg picture, and the average $\langle\cdots\rangle$ is evaluated by $(N/N_w) \times \sum_{n=1}^{N_w} \langle\Psi_n|\cdots|\Psi_n\rangle$, where N and N_w represent the number of molecules and

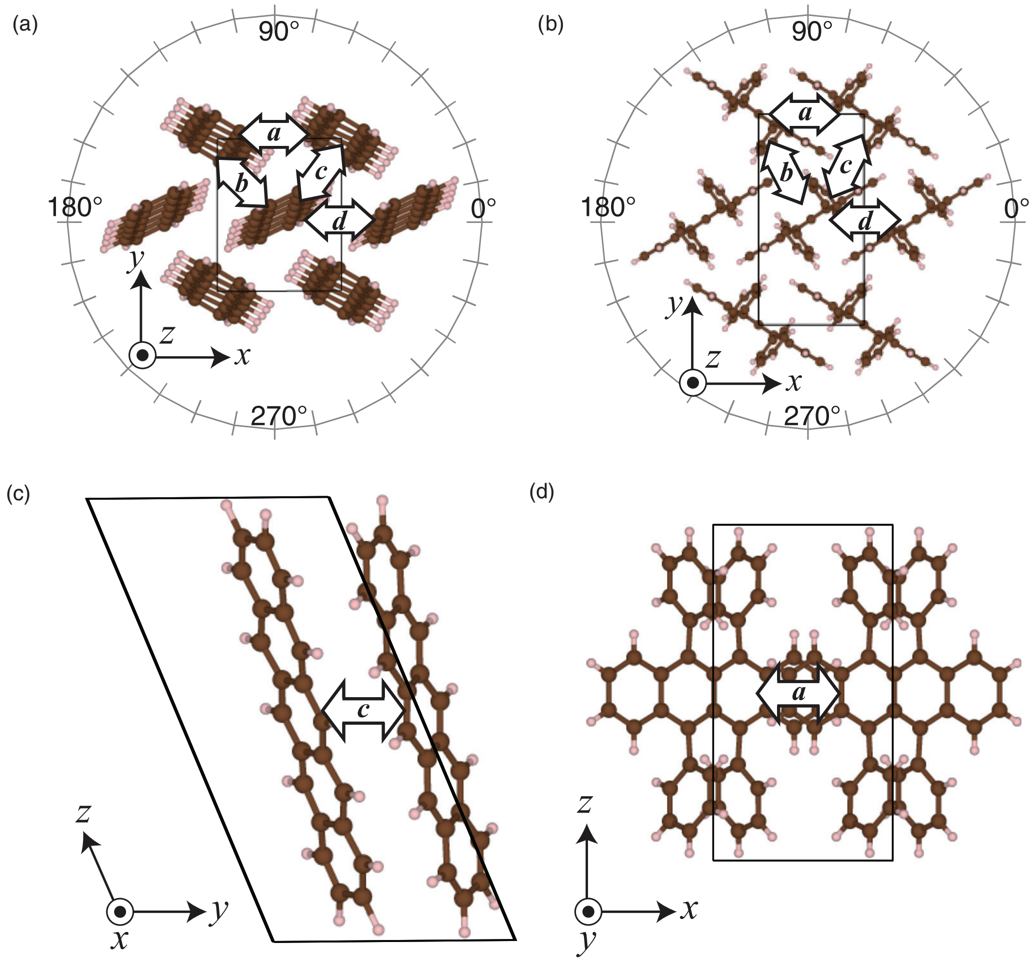

FIG. 1. (Color online) Crystal structures of pentacene in (a) the xy plane and (c) the yz plane and rubrene in (b) the xy plane and (d) the xz plane. The dimer, which is considered in order to numerically evaluate γ, α, and K by the dimer approach, is indicated by the arrow. The unit cell is represented by a box.

the number of initial wave packets, respectively. The use of random-phase wave packets for $|\Psi_n\rangle$, instead of using all the eigenvectors of $\hat{H}_e$, reduces the calculation cost. The carrier velocity v, mean-free path ℓ, and momentum-relaxation time τ, which are important in clarifying the transport characteristics, are obtained from $v_\xi = \lim_{t\to 0}\sqrt{D_\xi(t)/t}$, $\ell_\xi = D_\xi/v_\xi$, and $\tau_\xi = D_\xi/v_\xi^2$ with the diffusion coefficient D_ξ computed as the long-time limit of the time-dependent diffusion coefficient,

$$D_\xi(t) = \frac{1}{t}\frac{\displaystyle\int dE\, f(E)\langle \delta(E-\hat{H}_e)\{\hat{\xi}(t)-\hat{\xi}(0)\}^2\rangle}{\displaystyle\int dE\, f(E)\langle \delta(E-\hat{H}_e)\rangle}, \qquad (2)$$

as $\lim_{t\to+\infty} D_\xi(t)$.[22]

By performing real-time molecular dynamics simulations, we describe the intermolecular vibrations of organic molecular crystals. When the displacement of the nth molecular position at time t is represented by $\Delta\boldsymbol{R}_n(t)$, the motion of the nth molecule with mass M is given by the canonical equation of motion $M\,\Delta\ddot{\boldsymbol{R}}_n = -\partial E_{\mathrm{tot}}/\partial\,\Delta\boldsymbol{R}_n$, where $E_{\mathrm{tot}} \equiv \sum_{ij}\Delta E_{\mathrm{dim}}(\Delta R_{ij})$ is defined later. The temperature T is fixed with the normalization of kinetic energies of molecular vibrations at each time step under the condition $\sum_{n=1}^{N} M\,\Delta\dot{\boldsymbol{R}}_n(t)^2/2 = 3Nk_BT/2$, and the effects of intermolecular vibration on the electronic states are introduced as an ever-changing transfer energy $\gamma(t)$.[21]

We extract the transfer energy γ among adjacent molecules, electron-phonon (e-ph) coupling constant α, and elastic constant K from first-principles calculations based on density functional theory that includes the van der Waals interactions (DFT-D) approach[23] with the Becke three-parameter Lee-Yang-Parr (B3LYP) functional in conjunction with the 6-31G(d) basis set.[24] When we assume that the highest occupied molecular orbital (HOMO) and HOMO − 1 of the dimer are described in terms of only the HOMO of the monomers, we obtain the 2×2 secular equation $\boldsymbol{HC} = E\boldsymbol{SC}$, where $\boldsymbol{H}$ is the Hamiltonian matrix of the dimer with elements $H_{ij} \equiv \langle\Phi_i|\hat{H}|\Phi_i\rangle$ and $\boldsymbol{S}$ is the overlap matrix $S_{ij} \equiv \langle\Phi_i|\Phi_j\rangle$. Here, $|\Phi_i\rangle$ is the HOMO of the ith monomer. Applying Lödin's symmetric transformation, we obtain the effective Hamiltonian of the dimer. The off-diagonal element corresponds to the transfer energy between the monomers and is given by $\gamma_{ij} = \{2H_{ij} - (H_{ii}+H_{jj})S_{ij}\}/\{2(1-S_{ij}^2)\}$.[25]

Here, we treat single-crystal pentacene and rubrene, whose crystal structures are shown in Fig. 1. Note that even small molecular displacements induced by intermolecular vibrations

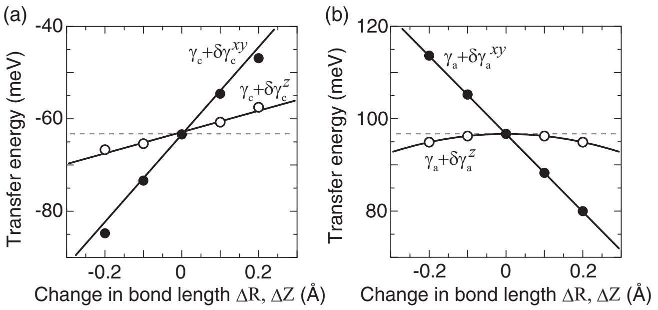

FIG. 2. (a) Calculated transfer energy γ_c as a function of change in bond length projected on the xy plane and along the z axis in the pentacene crystal. (b) Transfer energy γ_a as a function of change in bond length projected on the xy plane and along the z axis in the rubrene crystal.

TABLE I. Transfer energies γ, elastic constants K, and e-ph coupling constants for in-plane mode α^{xy} and out-of-plane mode α^z of single-crystal pentacene and rubrene.

	γ_a	γ_b	γ_c	γ_d	
Pentacene (meV)	27.1	30.2	−63.4	−2.3	
Rubrene (meV)	96.7	−15.9	−15.9	96.7	
	K_a	K_b	K_c	K_d	K_z
Pentacene (meV/Å^2)	417	1569	1777	603	1111
Rubrene (meV/Å^2)	522	427	427	522	1255
	α_a^{xy}	α_b^{xy}	α_c^{xy}	α_d^{xy}	
Pentacene (meV/Å)	22.4	16.7	94.6	18.7	
Rubrene (meV/Å)	84.3	29.5	29.5	84.3	
	α_a^{z}	α_b^{z}	α_c^{z}	α_d^{z}	
Pentacene (meV/Å)	−72.1	−60.4	23.1	−68.7	
Rubrene (meV/Å^2)	−44.5	13.5	13.5	−44.5	

lead to significant changes in transfer energy. As an example, we show the calculated transfer energy as a function of the change in bond length projected on the xy plane and along the z axis in the pentacene and rubrene crystals in Fig. 2. When the change in bond length between the ith and the jth molecules in the xy plane is $\Delta R_{ij}(t)$, the change in transfer energy is expressed by $\delta\gamma_{ij}^{xy}(t) = \alpha_{ij}^{xy}\Delta R_{ij}(t)$, where α_{ij}^{xy} is the e-ph coupling constant for the bond-length modulation. Furthermore, the molecular sliding affects the transfer energy in organic crystals with layer structures. When the displacement along the z axis is written as $\Delta Z_{ij}(t)$, the change in transfer energy is given by $\delta\gamma_{ij}^{z}(t) = \alpha_{ij}^{z}\Delta Z_{ij}(t)$ for pentacene and by $\delta\gamma_{ij}^{z}(t) = \alpha_{ij}^{z}\Delta Z_{ij}^2(t)$ for rubrene. As shown in Fig. 1, because the rubrene molecules are oriented perpendicular to the xy plane, the change in transfer energy along the z axis is symmetric with respect to $\Delta Z = 0$. In the pentacene crystals, on the other hand, the change in transfer energy is nearly antisymmetric, reflecting the inclined main axis of the molecules. The final form of the transfer energy is given by $\gamma_{ij}(t) = \gamma_{ij} + \delta\gamma_{ij}^{xy}(t) + \delta\gamma_{ij}^{z}(t)$. For the elastic constants, we evaluate the change in total energy of a dimer $\Delta E_{\mathrm{dim}}(\Delta R_{ij})$ as a function of ΔR_{ij}. Then, the elastic constant K_{ij} is obtained by fitting to the analytic expression $\Delta E_{\mathrm{dim}}(\Delta R_{ij}) = (1/2)K_{ij}\Delta R_{ij}^2$. Our molecular dynamics simulations show that the change in bond length projected on the xy plane reaches about 0.10–0.15 Å at 300 K, whereas, that along the z axis is a larger value of 0.2 Å in the case of pentacene. Note that, although this evaluation of K from the rigid dimer is a considerably simpler approach than the quasiharmonic lattice-dynamics method,[26] the obtained anisotropic molecular-vibration amplitude and its temperature dependence are quantitatively in good agreement with the experimental translation/libration/screw analysis of pentacene crystals.[27] However, it may be difficult to apply this approach of using a rigid molecule to molecules having thermally fluctuating side chains. We investigate the effects of not only bond-length modulation, but also molecular sliding. The disorder of transfer energy owing to the molecular sliding has similar energetic order to that owing to the bond-length modulation discussed in many previous reports.[15,28,29] In Table I, we show the obtained parameters of bonds a–d in Figs. 1(a) and 1(b). The DOS obtained from these parameters are in good agreement with the results of another theoretical study[30] as shown in Figs. 3(a) and 3(b). The size of the unit cell is 6.06 × 7.90 Å^2 for pentacene and 7.18 × 14.40 Å^2 for rubrene. We employ pentacene crystals of 300 × 250 unit cells with a mass of 4.616×10^{-25} kg and rubrene crystals of 500 × 300 unit cells with a mass of 8.850×10^{-25} kg. The charge density in the crystal is fixed at 10^{12} cm^{-2}. The dynamics calculations are performed using 40 initial conditions for up to 2 ps with $\Delta t \simeq 1$ fs for the evaluation of Eqs. (1) and (2).

First, we study the inverse effective mass since it is directly related to the carrier mobility in the effective-mass approximation. We obtain full band structures $E(\boldsymbol{k})$ using the parameters listed in Table I, and the hole effective mass m_ξ^* is obtained by fitting to the analytic expression $E(\boldsymbol{k}) \simeq E_0 - (\hbar^2/2m_\xi^*)(k_\xi - k_\xi^0)^2$ where the top of the HOMO band with energy E_0 is located at $k = k_\xi^0$ on the k_ξ axis. Figures 3(c)

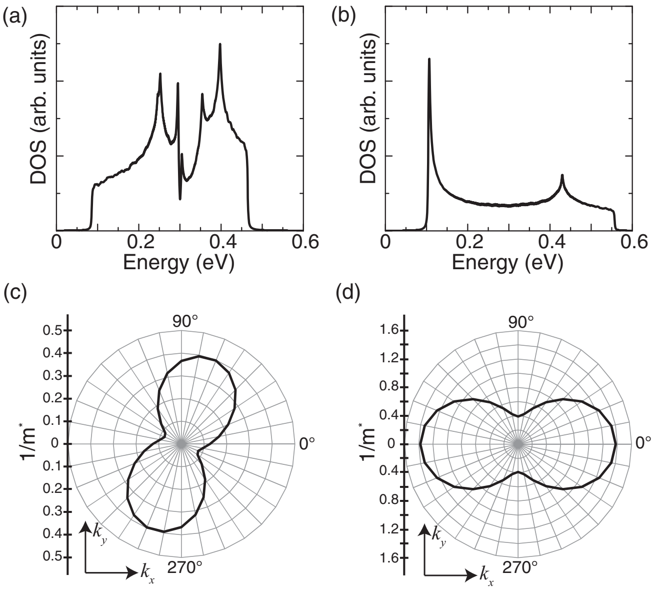

FIG. 3. Calculated DOS of the HOMO band of (a) pentacene and (b) rubrene crystals. Inverse of angle-resolved hole effective mass of (c) pentacene and (d) rubrene crystals.

and 3(d) show the inverse effective mass of single-crystal pentacene and rubrene in units of $1/m_e$, where m_e is the electron rest mass. The angles of the polar plot correspond to those labeled in Figs. 1(a) and 1(b). The effective mass sweeps out a smooth and symmetric curve with distinct maximum and minimum values, reflecting the transfer energies. Pentacene has a large effective mass, ranging from $2.5m_e$ to $12.5m_e$, compared with the rest mass, whereas, the effective mass of rubrene is smaller, ranging from only $0.73m_e$ to $2.6m_e$. These calculated values agree with experimental measurements by angle-resolved photoelectron spectroscopy, which reveal that the lightest effective masses of pentacene and rubrene crystals are $1.26m_e$ and $0.65m_e$, respectively.[31,32] The evaluation of the anisotropic ratio $m^*_{\rm max}/m^*_{\rm min}$ from the effective mass is 4.97 for pentacene and 3.53 for rubrene.

Next, we compare the effective mass with carrier mobilities. Figures 4(a) and 4(b) show polar plots for the mobilities μ of single-crystal pentacene and rubrene. Here, we assume that the charge carriers are scattered only by e-ph scattering to clarify the intrinsic charge transport properties of single crystals independent of extrinsic factors. The obtained mobilities with power-law temperature dependence signify the upper limit of the measurements in experiments. The anisotropic ratios of mobility $\mu_{\rm max}/\mu_{\rm min}$ are 3.94 for pentacene and 2.47 for rubrene at 300 K, which are consistent with several other experimental reports.[6,7,9] Although the mobility and inverse effective mass exhibit similar anisotropic characteristics, at first glance, the obtained anisotropic ratios of mobility are smaller than those of the effective mass. This implies that the simple effective-mass approximation is not sufficient for detailed analyses of anisotropic transport properties.

Figures 4(c) and 4(d) show the angle-resolved carrier velocities v. The magnitude of v for rubrene is about four times larger than that for pentacene. The anisotropy of the velocity resembles that of the inverse effective mass, reflecting the relationship of the velocity to the effective mass of $(1/2)m^*v^2 \simeq (3/2)k_BT$. On the other hand, the anisotropy of the momentum-relaxation time is entirely different from that of the carrier velocity as shown in Figs. 4(e) and 4(f). We find a strong anisotropy of τ, which deviates significantly from the isotropic τ assumed in some previous studies. The magnitude of the momentum-relaxation time is maximum along the direction where the mobility takes a minimum. The ratio $\tau_{\rm min}/\tau_{\rm max}$ is ~0.6 for both pentacene and rubrene independent of the temperature. To understand these anisotropic behaviors of τ, we consider the changes in transfer energy γ owing to dynamical disorder since the carrier scattering rates are roughly estimated from Fermi's golden rule $1/\tau \propto |\delta\gamma|^2$. In the rubrene crystals at 300 K, for example, the dynamical disorder induces anisotropic transfer energies, such as $\delta\bar{\gamma}_{a(d)} \simeq$ 18 and $\delta\bar{\gamma}_{b(c)} \simeq 6.5$ meV. As a result, τ becomes small along the a direction. Furthermore, on comparing τ for pentacene and rubrene, we find that the carrier scattering rates are larger in rubrene crystals than in pentacene, although rubrene exhibits higher mobilities. Since the relaxation time τ is large in the low-velocity direction, the mean-free path $\ell(=v \times \tau)$ becomes less anisotropic and is moderated. This explains the polar plots of ℓ shown in (g) and (h) where ℓ appears to be less anisotropic. It should be noted that a more isotropic mean-free path of rubrene is realized as a result of a sensitive balance between the anisotropic intermolecular electronic couplings and the intermolecular vibrations.

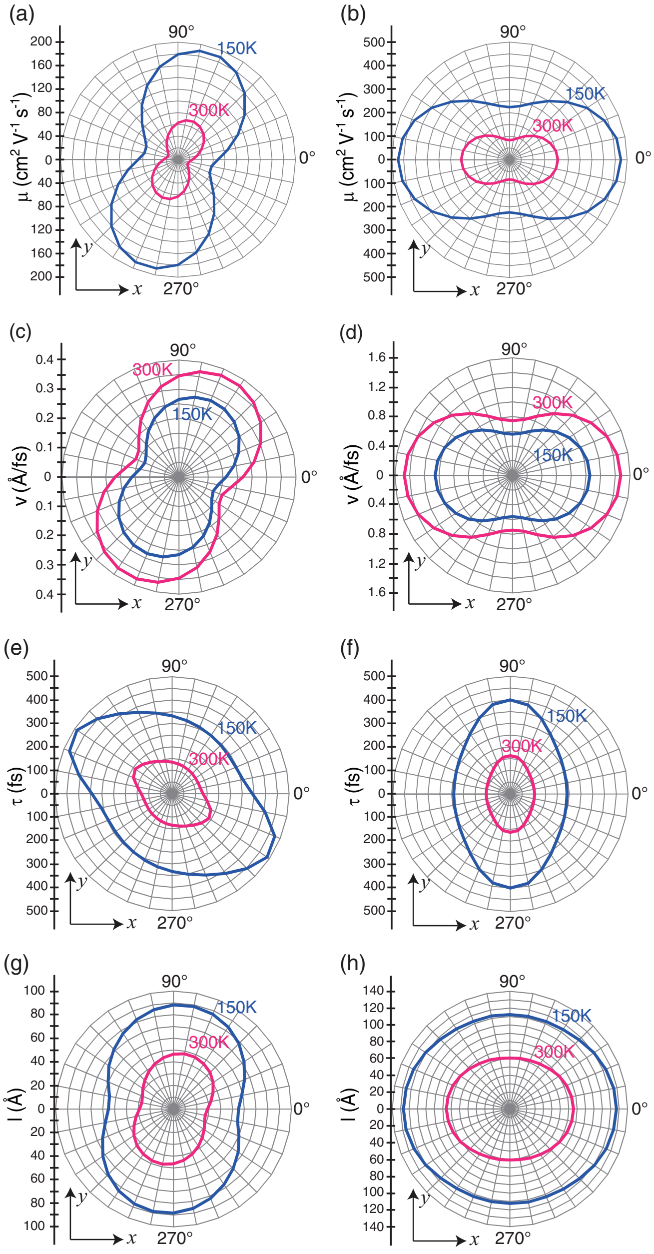

FIG. 4. (Color online) (a) Angle-resolved mobilities, (c) charge-carrier velocities, (e) momentum-relaxation times, and (g) mean-free paths of single-crystal pentacene at 150 and 300 K. Those of single-crystal rubrene are shown in (b), (d), (f), and (h).

Figure 5(a) shows the power-law temperature dependence of the mobilities of pentacene and rubrene single crystals. The filled and open circles (triangles), respectively, represent the maximum and minimum μ of rubrene (pentacene). The exponent n of the T^{-n} dependence decreases from 1.76 to 1.22 with increasing mobility. Nevertheless, the exact value of n is a rather sensitive function of anisotropy and bandwidth;[33] there is a similarity between our result and those of the theoretical studies by Troisi[20] and Fratini and Ciuchi,[34] who suggested

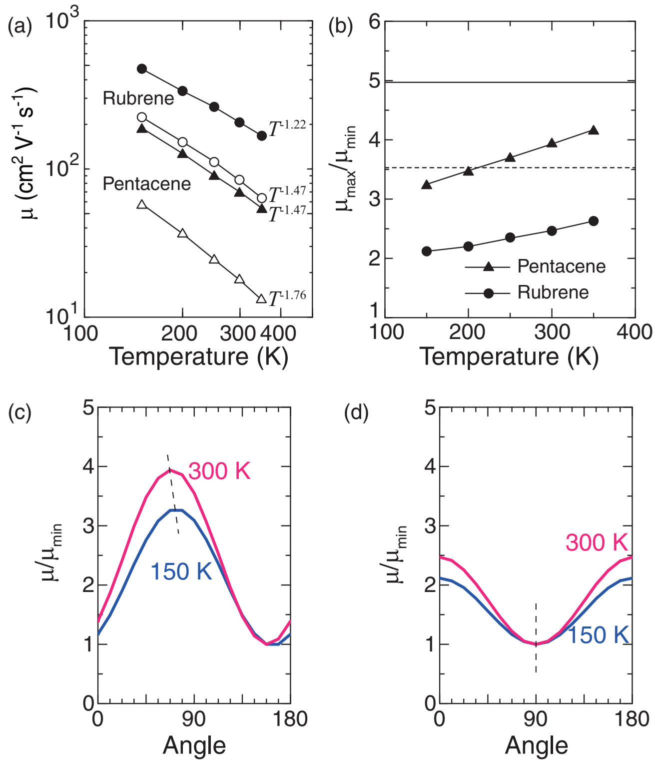

FIG. 5. (Color online) (a) Logarithmic plot of mobility μ as a function of temperature. The filled and open circles, respectively, represent the maximum and minimum μ of rubrene, whereas, the triangles represent those of pentacene. The power-law exponents of pentacene and rubrene range between -1.22 and -1.76 at around room temperature. (b) Temperature dependence of ratio $\mu_{\mathrm{max}}/\mu_{\mathrm{min}}$ of single-crystal pentacene (solid circles) and rubrene (open circles). For comparison, the ratio $m^*_{\mathrm{max}}/m^*_{\mathrm{min}}$ is shown for pentacene (solid line) and rubrene (broken line). The anisotropic ratio of μ to μ_{min} as a function of the angle is shown for (c) pentacene and (d) rubrene at 150 and 300 K.

that the computed decrease in the mobility with increasing T is intermediate between $\mu \propto T^{-2}$ and $\mu \propto T^{-1}$ because of the simultaneous presence of band states and incoherent states. Then, we investigate the temperature dependence of the anisotropic ratio of mobilities $\mu_{\mathrm{max}}/\mu_{\mathrm{min}}$ for pentacene and rubrene as shown in Fig. 5(b). We see that these are distinctly temperature dependent and are smaller values than those of the effective-mass ratio in the whole temperature regime discussed here. The mobility ratio becomes large as the temperature increases, whereas, the behaviors of $\tau_{\mathrm{min}}/\tau_{\mathrm{max}}$ are independent of temperature. Since the mobility is proportional to the diffusion coefficient $D_\xi = v_\xi^2 \tau_\xi$, the temperature dependence of the mobility ratio is due to the different temperature dependences of the carrier velocity. Also, as shown in Figs. 5(c) and 5(d), the main axis of the mobility tensor for pentacene rotates slightly with temperature owing to the anisotropic e-ph coupling, whereas, there is no rotation for rubrene since rubrene crystals are symmetric with respect to the main axis of the mobility.

To summarize, using the quantum wave-packet dynamics coupled with the classical molecular dynamics, we studied the realistic intermolecular-vibration (lattice-phonon) effects on the anisotropic transport properties of pentacene and rubrene single-crystal organic semiconductors via systematic evaluations of the angle-resolved effective mass, mobility, carrier velocity, momentum-relaxation time, and mean-free path. We found that intermolecular vibrations induce a strongly anisotropic momentum-relaxation time but moderate the anisotropy of carrier mobility, which increases with temperature much more than that of the inverse effective mass. We also found that the main axis of the mobility tensor rotates slightly with temperature in pentacene crystals. These results clarify the mechanism of the deviation of the anisotropic ratio of mobility from that of effective mass observed in experiments.

We thank J. Takeya and T. Uemura for valuable suggestions. Financial support was provided by JST-PRESTO “Molecular technology and creation of new functions” and JSPS KAKENHI Grants No. 24760024 and No. 23360018. Numerical calculations were performed at the Supercomputer Center, ISSP, University of Tokyo and the Center for Computational Sciences, University of Tsukuba.

---

[*] ishii@bk.tsukuba.ac.jp

[1] S. F. Nelson, Y.-Y. Lin, D. J. Gundlach, and T. N. Jackson, Appl. Phys. Lett. **72**, 1854 (1998).
[2] V. Podzorov, E. Menard, A. Borissov, V. Kiryukhin, J. A. Rogers, and M. E. Gershenson, Phys. Rev. Lett. **93**, 086602 (2004).
[3] J. Takeya, M. Yamagishi, Y. Tominari, R. Hirahara, Y. Nakazawa, T. Nishikawa, T. Kawase, T. Shimoda, and S. Ogawa, Appl. Phys. Lett. **90**, 102120 (2007).
[4] J. H. Burroughes, D. D. C. Bradley, A. R. Brown, R. N. Marks, K. Mackay, R. H. Friend, P. L. Burns, and A. B. Holmes, Nature (London) **347**, 539 (1990).
[5] C. W. Tang, Appl. Phys. Lett. **48**, 183 (1986).
[6] V. C. Sundar, J. Zaumseil, V. Podzorov, E. Menard, R. L. Willett, T. Someya, M. E. Gershenson, and J. A. Rogers, Science **303**, 1644 (2004).
[7] J. Y. Lee, S. Roth, and Y. W. Park, Appl. Phys. Lett. **88**, 252106 (2006).
[8] O. Ostroverkhova, D. G. Cooke, F. A. Hegmann, R. R. Tykwinski, S. R. Parkin, and J. E. Anthony, Appl. Phys. Lett. **89**, 192113 (2006).
[9] C. Reese and Z. Bao, Adv. Mater. **19**, 4535 (2007).
[10] A. Saeki, S. Seki, T. Takenobu, Y. Iwasa, and S. Tagawa, Adv. Mater. **20**, 920 (2008).
[11] M. Uno, Y. Tominari, M. Yamagishi, I. Doi, E. Miyazaki, K. Takimiya, and J. Takeya, Appl. Phys. Lett. **94**, 223308 (2009).
[12] R. C. Hatch, D. L. Huber, and H. Höchst, Phys. Rev. B **80**, 081411(R) (2009).
[13] G. A. de Wijs, C. C. Mattheus, R. A. de Groot, and T. T. M. Palstra, Synth. Met. **139**, 109 (2003).
[14] K. Hummer and C. Ambrosch-Draxl, Phys. Rev. B **72**, 205205 (2005).
[15] H. Yoshida and N. Sato, Phys. Rev. B **77**, 235205 (2008).
[16] S. Yin and Y. Lv, Org. Electron. **9**, 852 (2008).
[17] S.-H. Wen, A. Li, J. Song, W.-Q. Deng, K.-L. Han, and W. A. Goddard III, J. Phys. Chem. B **113**, 8813 (2009).

[18] V. Stehr, J. Pfister, R. F. Fink, B. Engels, and C. Deibel, Phys. Rev. B **83**, 155208 (2011).

[19] F. Ortmann, F. Bechstedt, and K. Hannewald, Phys. Status Solidi B **248**, 511 (2011).

[20] A. Troisi, J. Chem. Phys. **134**, 034702 (2011).

[21] H. Ishii, K. Honma, N. Kobayashi, and K. Hirose, Phys. Rev. B **85**, 245206 (2012).

[22] H. Ishii, N. Kobayashi, and K. Hirose, Appl. Phys. Express **1**, 123002 (2008); Phys. Rev. B **82**, 085435 (2010).

[23] S. Grimme, J. Comput. Chem. **25**, 1463 (2004).

[24] We used the GAMESS program at the DFT-D/B3LYP-D3/6-31G(d) level: M. W. Schmidt, K. K. Baldridge, J. A. Boatz, S. T. Elbert, M. S. Gordon, J. H. Jensen, S. Koseki, N. Matsunaga, K. A. Nguyen, S. J. Su, T. L. Windus, M. Dupuis, and J. A. Montgomery, Jr., J. Comput. Chem. **14**, 1347 (1993).

[25] E. F. Valeev, V. Coropceanu, D. A. da Silva Filho, S. Salman, and J.-L. Brédas, J. Am. Chem. Soc. **128**, 9882 (2006).

[26] A. Girlando, L. Grisanti, M. Masino, I. Bilotti, A. Brillante, R. G. Della Valle, and E. Venuti, Phys. Rev. B **82**, 035208 (2010).

[27] T. Fukami, H. Ishii, N. Kobayashi, T. Uemura, J. Takeya, and K. Hirose (unpublished).

[28] J. H. Kang, D. da Silva Filho, J.-L. Bredas, and X.-Y. Zhu, Appl. Phys. Lett. **86**, 152115 (2005).

[29] A. Troisi, G. Orlandi, and J. E. Anthony, Chem. Mater. **17**, 5024 (2005).

[30] L. Tsetseris and S. T. Pantelides, Eur. Phys. J.: Appl. Phys. **46**, 12511 (2009).

[31] H. Kakuta, T. Hirahara, I. Matsuda, T. Nagao, S. Hasegawa, N. Ueno, and K. Sakamoto, Phys. Rev. Lett. **98**, 247601 (2007).

[32] S.-I. Machida, Y. Nakayama, S. Duhm, Q. Xin, A. Funakoshi, N. Ogawa, S. Kera, N. Ueno, and H. Ishii, Phys. Rev. Lett. **104**, 156401 (2010).

[33] S. H. Glarum, J. Phys. Chem. Solids **24**, 1577 (1963).

[34] S. Fratini and S. Ciuchi, Phys. Rev. Lett. **103**, 266601 (2009).